Angewandte Chemie
Eine Zeitschrift der Gesellschaft Deutscher Chemiker

Supporting Information

69451 Weinheim, Germany

Reaction Dynamics of the Decaniobate ($[H_xNb_{10}O_{28}]^{(6-x)-}$) Ion in Water

*Eric M. Villa, C. André Ohlin, Edina Balogh, Travis M. Anderson, May D. Nyman, and William H. Casey**

[*] Mr. Eric M. Villa, Dr. C. André Ohlin, Dr. Edina Balogh, Prof. William H. Casey
Department of Chemistry and Department of Geology
University of California, Davis, CA 95616
Fax: (+) 1 530-752-8995
E-mail: whcasey@ucdavis.edu
Homepage: http://chemgroups.ucdavis.edu/~casey/
Dr. Travis M. Anderson, Dr. May D. Nyman,
Geochemistry Division
Sandia National Laboratories
Albuquerque, NM 87185

S.1 Synthesis

A 3.5 g sample of $[N(CH_3)_4]OH•5H_2O$ and 1.3 g of $^{17}OH_2$ (40% ^{17}O) were added to 50 mL of anhydrous ethanol; the mixture was stirred until a clear solution was obtained, and then 6.35 g of $Nb(OCH_2CH_3)_5$ was added in approximately ~0.8 mL aliquots with vigorous stirring. The mixture was refluxed for 10 h, cooled to room temperature, and filtered. The resulting product was washed with 50 mL of ethanol. The solid was redissolved by adding it in small aliquots to 15 mL of warm methanol. The solution was filtered warm through a 0.45 µm syringe filter, and 1.93 g of crystalline $[N(CH_3)_4]_6[Nb_{10}O_{28}]•6H_2O$ was obtained by slow evaporation of the solution contained in a 125 mL Erlenmeyer flask at 0°C over several days (50% yield based on Nb).

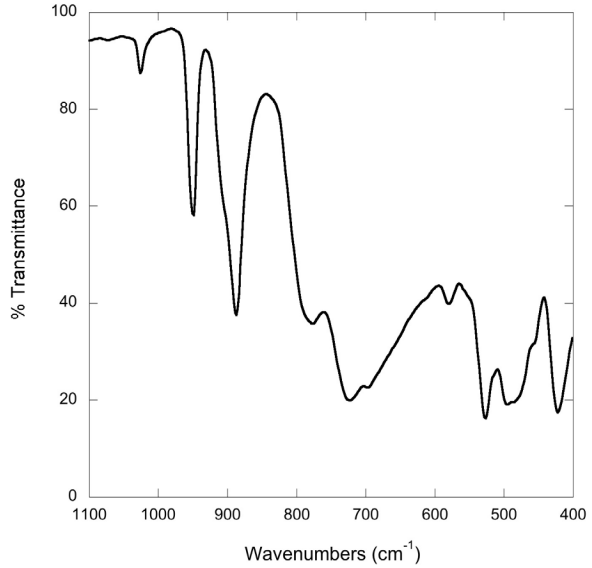

Figure S.1.1 Infrared spectrum of the crystalline $[(CH_3)_4N]_6Nb_{10}O_{28}•6\ H_2O$ used in this study. The purity of the compound was confirmed by a band-for-band match with the spectrum reported by Graeber and Morosin [5].

To make the $[(CH_3)_4N]_8Nb_6O_{19}$ for ESI-MS**,** a 0.94 g sample of $[(CH_3)_4N]_6Nb_{10}O_{28}•6H_2O$ was dissolved in 8 mL of H_2O and 0.87 g of $(CH_3)_4N(OH)•5H_2O$ was added with vigorous stirring for 1 h. The solution was added to 200 mL of CH_3CN in a 500 mL beaker and manually stirred with a metal spatula for several minutes. The liquid was decanted, leaving a viscous residue on the sides of the beaker. An additional 200 mL of CH_3CN was added and the process was repeated several times until a white powder was

obtained. The hygroscopic solid is dried under vacuum for 24 h. Both ESI-MS and ^{17}O-NMR indicate that the compound is pure.

S.2 NMR Spectroscopy and Rate Measurements

The solution-state ^{17}O-NMR experiments were conducted with a Bruker Avance spectrometer located at the UCD NMR facility. This spectrometer is based on an 11.7T magnet (ν_o=67.8 MHz for ^{17}O) and is fitted with a 10-mm broadband probe. The ^{17}O-NMR spectra were taken with single-pulse excitation using 20 μs pulses ($\frac{\pi}{2} \approx 40\ \mu s$) and recycle delays of 6 ms. Depending upon the sample concentration and rate of reaction, 1,000-15,000 acquisitions were required to establish an adequate signal-to-noise ratio. The time-domain data were digitized at 100 kHz. We employed a 0.3 M $TbCl_3$ solution as an external intensity standard, which was included in the 10 mm NMR tube as a coaxial insert. The temperature was measured by replacing the sample with a copper-constantan thermocouple fitted into an NMR tube. The accuracy of the measured temperature was about ±0.1^{o}C. Peak positions are reported relative to the bulk water peak, which was assigned to 0 ppm.

Assignment of ^{17}O NMR signals is straightforward. These assignments were based on the work of Marek [1] which in turn is based on similar work on $[V_{10}O_{28}]^{6-}$ and other isopolyoxometalate ions[2]. These studies show that the ^{17}O signals are shifted up field with increased coordination number. The three types of μ_2-O in the decaniobate ion could be distinguished by signal area, as they represent 2, 4 and 8 oxygens, respectively. Integration could not be used to assign the two types of η-O, so DFT calculations were used instead as discussed in Section S.3, below.

Table S-2-1: Buffers used to control pH in the oxygen-isotope-exchange experiments. The final pH was reached by dropwise addition of $[N(CH_3)_4]OH$ and/or HCl. All buffers were prepared with a 0.1 M $[N(CH_3)_4]Cl$ background electrolyte.

pH	Buffer composition
5. 5, 6.0, 6.6	10 mM MES: 2-(*N*-morpholino)ethanesulfonic acid
7.1, 7.5	10 mM PIPES: Piperazine-1,4-bis(2-ethanesulfonic acid)
8.0, 8.5	10 mM HEPES: *N*-(2-hydroxyethyl)piperazine-*N*′-(2-ethanesulfonic acid)
8.7, 8.8	10 mM TRIS: 2-Amino-2-hydroxymethyl-1,3-propanediol
9.3	100 mM H_3BO_3

Table S-2-2: Experimental conditions and rates of steady oxygen-isotope exchange into sites in the $[H_xNb_{10}O_{28}]^{(6-x)-}$ ion as measured by ^{17}O NMR. Rates corresponding to Site **A**, the μ_6-oxo, indicate rates of dissociation of the molecule. Activation parameters correspond to pH=6.6 for steady isotopic exchange of oxygens.

Temp[1] (°C)	pH	$[TMA_6Nb_{10}O_{28}]$[2] (mM)	log(k) s^{-1} μ_6-oxo (Site **A**)	log(k) s^{-1} μ_3-oxo (Site **B**)	log(k) s^{-1} μ_2-oxo (Site **C**)	log(k) s^{-1} μ_2-oxo (Site **D**)	log(k) s^{-1} μ_2-oxo (Site **E**)	log(k) s^{-1} η=O (Site **F**)	log(k) s^{-1} η=O (Site **G**)
35.5	5.5_0	5.41	--	-7.16 ± 0.07	-5.51 ± 0.02	-3.68 ± 0.04	-6.63 ± 0.05	-3.58 ± 0.04	-3.46 ± 0.02
35.5	6.0_5	5.36	--	-7.07 ± 0.04	-5.69 ± 0.03	-3.98 ± 0.04	-6.59 ± 0.02	-4.01 ± 0.04	-3.82 ± 0.02
35.5	6.6_2	5.82	--	-7.19 ± 0.03	-5.71 ± 0.02	-4.13 ± 0.04	-6.67 ± 0.02	-4.47 ± 0.04	-4.12 ± 0.02
35.5	7.1_1	5.57	--	-7.38 ± 0.06	-5.74 ± 0.02	-4.15 ± 0.04	-6.74 ± 0.02	-4.52 ± 0.04	-4.25 ± 0.02
35.5	7.5_1	5.67	-7.80 ± 0.08	-7.30 ± 0.02	-5.62 ± 0.02	-3.87 ± 0.04	-6.71 ± 0.01	-4.64 ± 0.04	-4.21 ± 0.02
35.5	8.0_8	5.00	-7.04 ± 0.02	-6.79 ± 0.02	-5.30 ± 0.02	-3.50 ± 0.04	-6.37 ± 0.01	-4.47 ± 0.04	-3.73 ± 0.02
35.5	8.4_9	4.61	-6.79 ± 0.01	-6.53 ± 0.02	-4.99 ± 0.02	-2.83 ± 0.04	-6.16 ± 0.01	-4.41 ± 0.04	-3.46 ± 0.02
35.5	9.3_1	10.08	-4.99 ± 0.01	-4.74 ± 0.01	-3.91 ± 0.02	-2.12 ± 0.13	-4.60 ± 0.01	-3.68 ± 0.04	-2.52 ± 0.04
51.6	6.6_1	5.31	--	-6.90 ± 0.03	-4.96 ± 0.02	-3.62 ± 0.04	-6.23 ± 0.01	-3.89 ± 0.04	-3.65 ± 0.02
45.3	6.6_1	5.31	--	-7.01 ± 0.04	-5.24 ± 0.02	-3.84 ± 0.04	-6.40 ± 0.02	-4.13 ± 0.04	-3.82 ± 0.02
40.2	6.6_1	4.97	--	-7.03 ± 0.05	-5.48 ± 0.02	-4.06 ± 0.04	-6.49 ± 0.02	-4.37 ± 0.04	-4.00 ± 0.02
35.5	6.6_1	10.52	--	-7.17 ± 0.04	-5.68 ± 0.02	-4.22 ± 0.04	-6.64 ± 0.02	-4.42 ± 0.04	-4.15 ± 0.02
35.5	6.6_1	7.77	--	-7.17 ± 0.04	-5.71 ± 0.02	-4.19 ± 0.04	-6.65 ± 0.02	-4.50 ± 0.04	-4.14 ± 0.02
ΔH‡ ($kJ \cdot mol^{-1}$)	6.6		----	28.4(± 6.7)	86.4(±0.6)	61.2(±7.6)	48.0(±4.2)	68.6(±6.5)	54.2(±2.18)
ΔS‡ ($J \cdot mol^{-1}K^{-1}$)	6.6			-290(±21)	-74.4(±2)	-126.7(±24)	-217(±13)	-109 (±20.2)	-148.6(±6.6)

[1]Uncertainties in temperature are ±0.2°C, save the sample at 40.2°C where the uncertainty was ±0.5°C.
[2]Uncertainties in the concentrations are ±1%.
Uncertainties in all other parameter are estimated as the error of the regression or the standard deviation of repeated trials, whichever is larger.

S.3 Density Functional (DFT) Calculations

Electronic-structure calculations were conducted using the Gaussian 03 code [3] and a 20-processor home-built parallel-processing computer. The all-electron DGDZVP basis set was employed. In all cases we used the B3LYP hybrid functional and the PCM solvent model, which ensured electronic stability [4]. Unless otherwise noted, all structures are fully stable in normal-mode vibrational analysis, which employed analytical second derivatives of energy.

Table S-3-1: DFT-calculated total free energies in solution using the PCM model for a dielectric medium, including all non-electrostatic terms, and an all-electron basis set (DGDZVP/B3LYP/PCM).

Molecule	Energy Hartrees	Proton Affinities $kJ \cdot mol^{-1}$	Zero-Point Energies; $kJ \cdot mol^{-1}$
$Nb_{10}O_{28}^{6-}$	-39662.388505	0	252.
O_B-$HNb_{10}O_{28}^{5-}$	-39662.837522	-1151.	279.5
[1]O_C-$HNb_{10}O_{28}^{5-}$	-39662.837546	-1154.	277.
O_D-$HNb_{10}O_{28}^{5-}$	-39662.836635	-1152.	277.
O_E-$HNb_{10}O_{28}^{5-}$	-39662.827663	-1128.	277.
O_F-$HNb_{10}O_{28}^{5-}$	-39662.841856	-1166.	276.
[1]O_G-$HNb_{10}O_{28}^{5-}$	-39662.830960	-1139.	274.
$V_{10}O_{28}^{6-}$	-11548.052825	0	277.
O_B-$HV_{10}O_{28}^{5-}$	-11548.520033	-1194.	309.
[1]O_C-$HV_{10}O_{28}^{5-}$	-11548.514283	-1181.	308.
O_D-$HV_{10}O_{28}^{5-}$	-11548.508339	-1164.	308.
O_E-$HV_{10}O_{28}^{5-}$	-11548.505815	-1157.	309.
O_F-$HV_{10}O_{28}^{5-}$	-11548.504804	-1157.	306.
O_G-$HV_{10}O_{28}^{5-}$	-11548.497320	-1139.	305.

[1]Imaginary frequencies exist in the optimized structures. For **Sites C and G** in the $HNb_{10}O_{28}^{5-}$ ion the imaginary frequencies are -373 cm^{-1} and -202 cm^{-1}, respectively. These are sufficiently high to probably be a real manifestations of the potential-energy surface and not an artefacts of optimization. For **Site C** in the $HV_{10}O_{28}^{5-}$ ion the imaginary frequency is -90 cm^{-1} and it is not clear if this is significant.

S.4: ESI-MS and ^{17}O-NMR Identification of Dissociation Products

We present negative-ion electrospray ionization mass spectra (ESI-MS) and ^{17}O-NMR data in this section. Positive-ion ESI-MS spectra were also collected, but were not helpful.

Figure S-4-1: The appearance of ^{17}O-NMR signals unrelated to sites in the $[H_xNb_{10}O_{28}]^{(6-x)-}$ corresponds to the formation of ^{17}O-enriched dissociation products. This is so because we dissolve ^{17}O-enriched $[H_xNb_{10}O_{28}]^{(6-x)-}$ salt into isotopically normal water. **(A)** Dissociation creates a heptaniobate fragment. Dissociation of ^{17}O-enriched decaniobate (50 mg) in 2 mL of isotopically normal water at pH~12.5 and 308.5 K as a function of time. The circled peaks correspond to μ_2-, μ_3-, and μ_6-oxygens in a heptaniobate ion. Hexaniobate η=O, μ_2-O, and μ_6-oxygens are identified. The times correspond to 650, 2600, 4550, 6900 and $1.82 \cdot 10^6$ s. For reasons of clarity, the spectrum of the solution before addition of base, which showed the $[Nb_{10}O_{28}]^{6-}$ ion, was omitted.

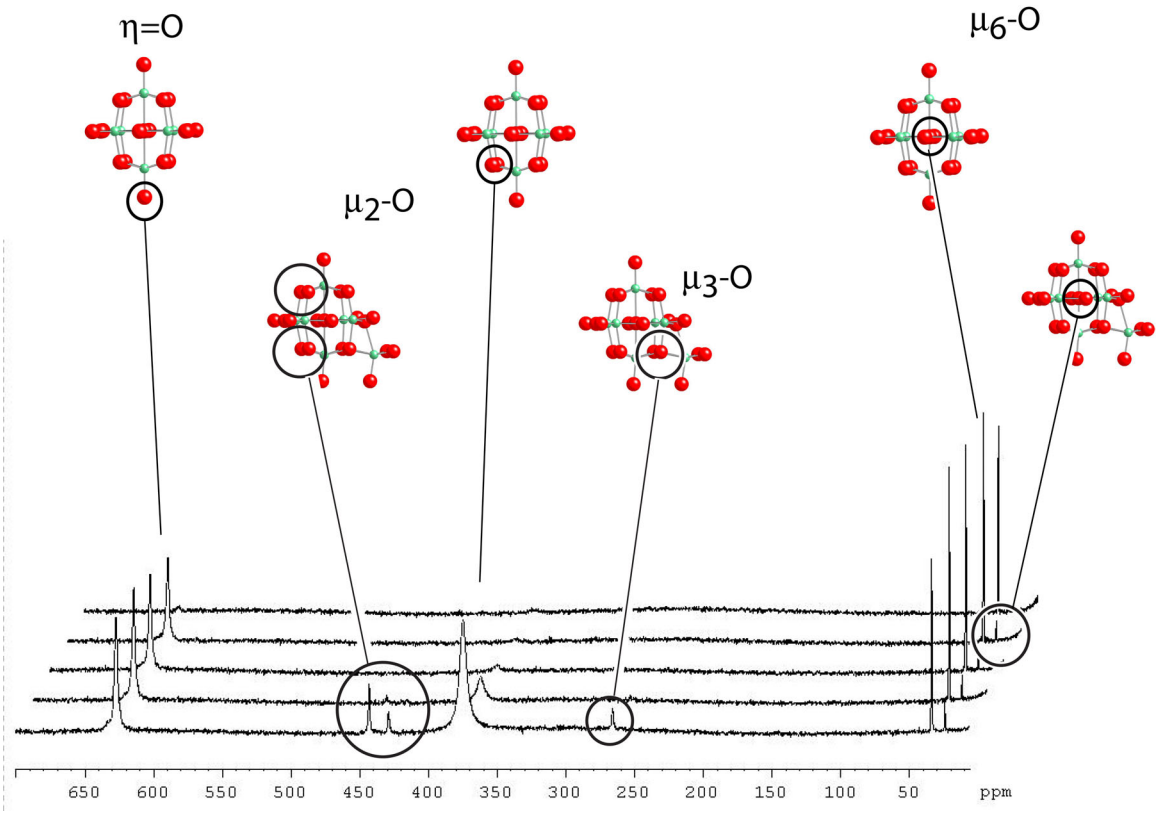

Figure S-4-2: Stacked plots of the 400-500 m/z region of the ESI-MS spectra taken with 3 minute intervals (0-70 min.). Insets show the effect of ^{18}O-enrichment (blue) on the peak patterns. Acquired using 75 µM $[N(CH_3)_4]_6[Nb_{10}O_{28}]$ at pH 11.15.

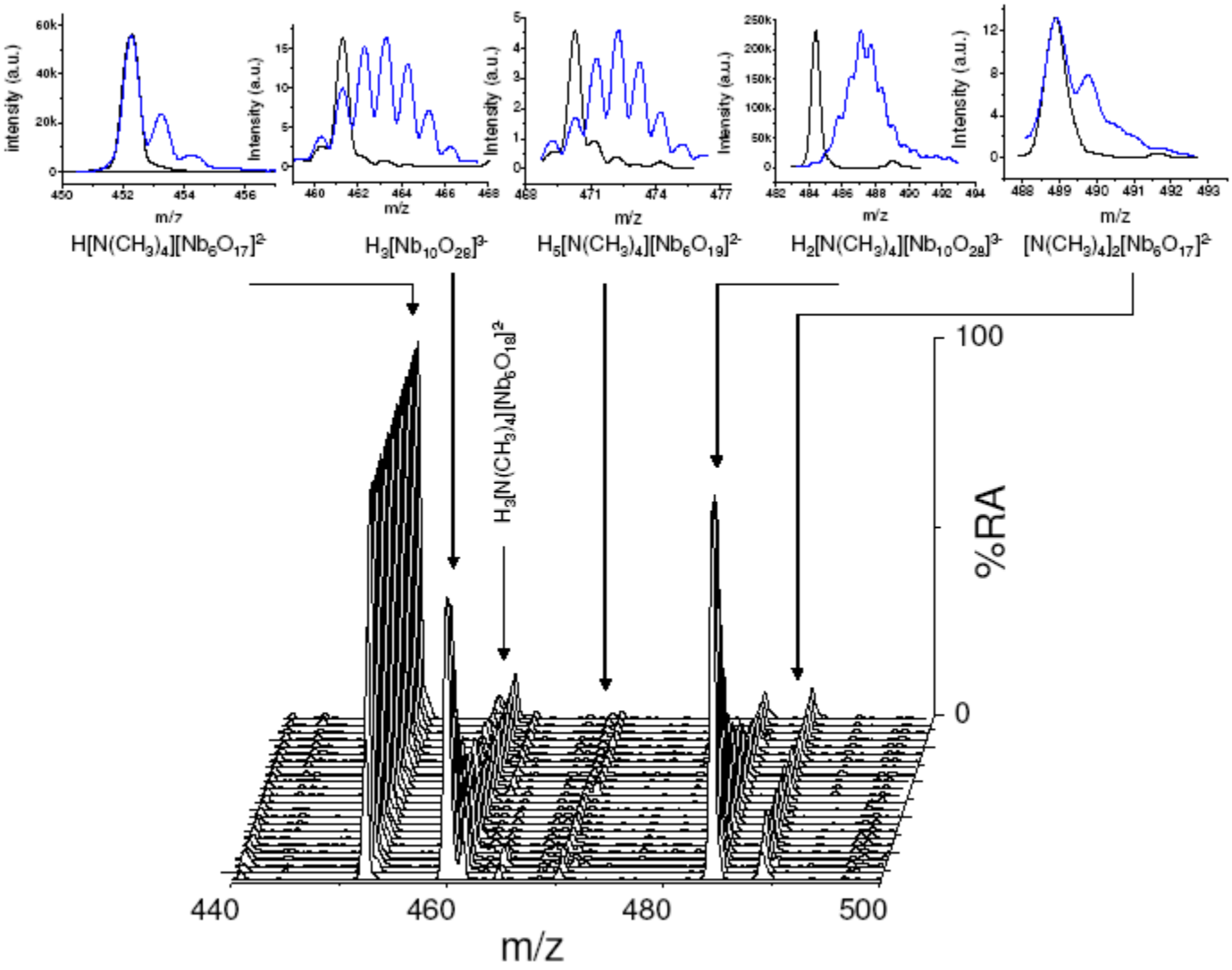

Figure S-4-3: Expansion of the ESI-MS data in the 520-600 m/z region, showing peaks assigned to different heptaniobate ions. Inset shows isotope pattern for isotopically normal (black) and ^{18}O-enriched (blue) ions. Acquired using 75 μM $[N(CH_3)_4]_6[Nb_{10}O_{28}]$ at pH 11.15

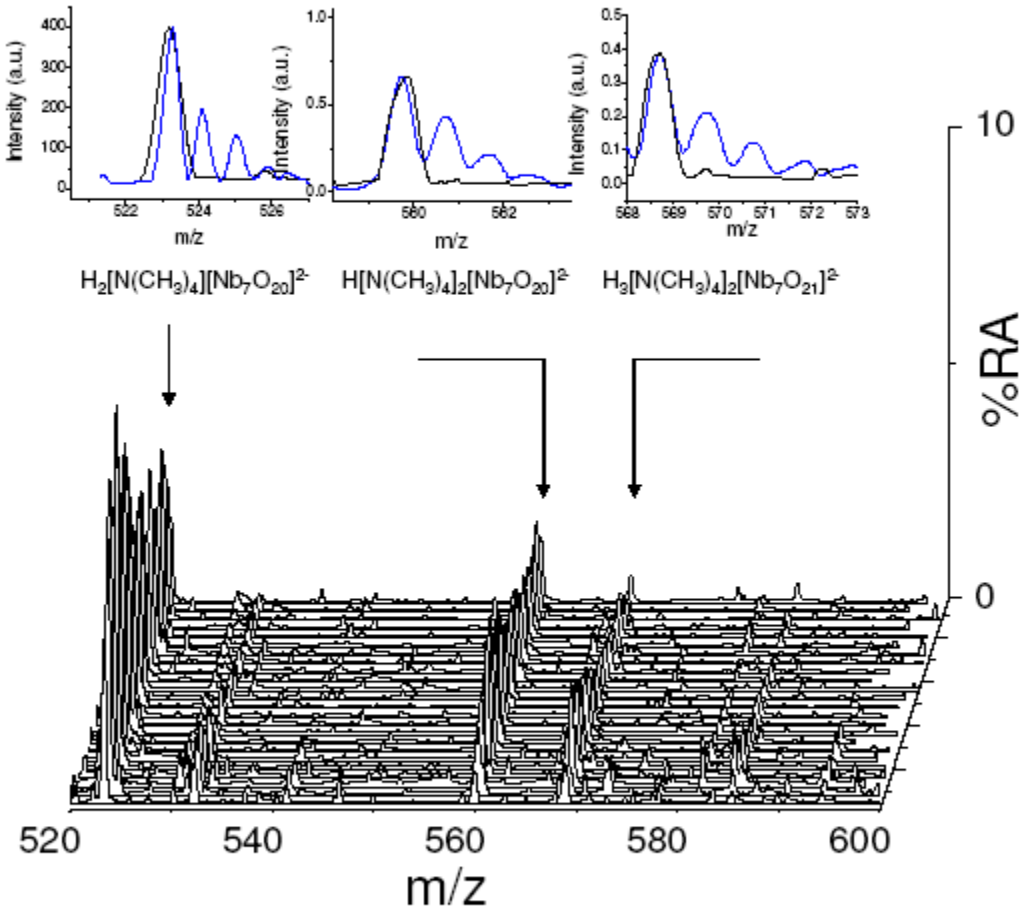

Figure S-4-4: Variation in abundance of selected ESI-MS peaks as a function of time. The disruption at 40 minutes are due to change of syringes.

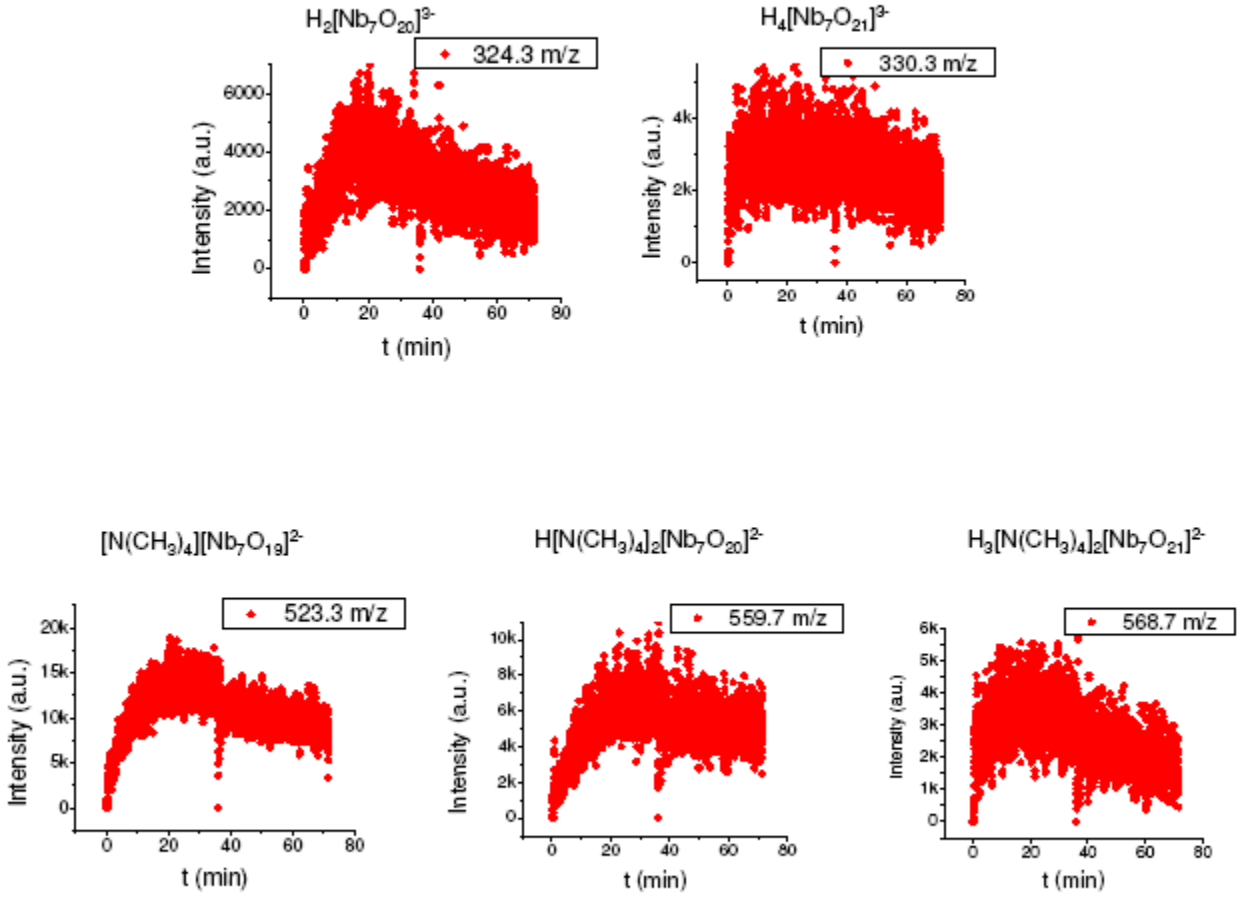

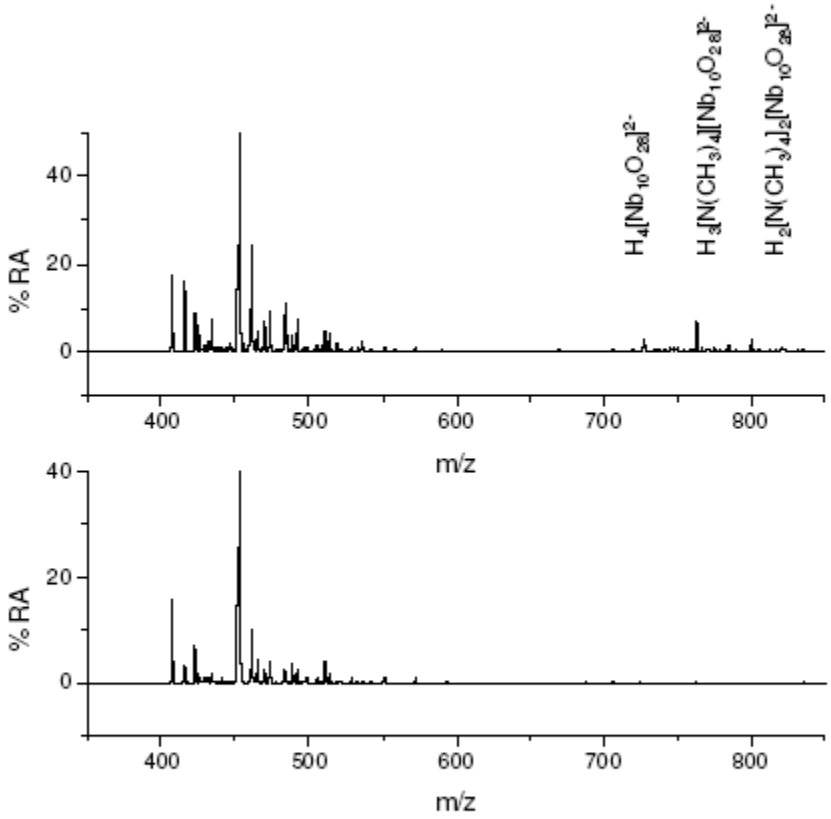

Figure S-4-5: ESI-MS spectra of $[N(CH_3)_4]_8[Nb_6O_{19}]$ in a borate buffer (pH 7.82, $[[Nb_6O_{19}]^{8-}]$=28 mM, $[B(OH)_3]$=888 mM, $[N(CH_3)_4]$=185 mM) after 1 minute (bottom) and 20 hours (top). Samples were diluted 100-fold before analysis. %RA stands for percentage relative abundance.

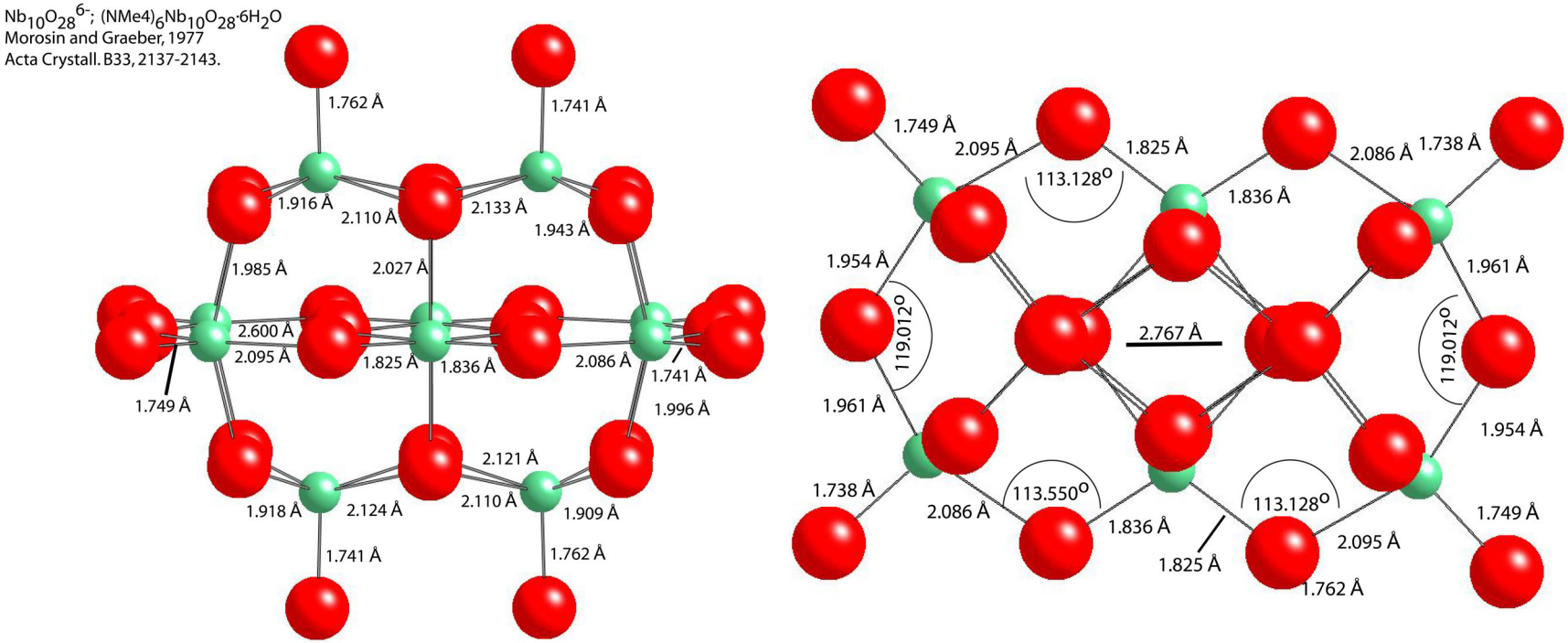

Figure S-5-1: X-ray structural information about the [$Nb_{10}O_{28}^{6-}$] ion from Morosin and Graeber (1977), who crystallized the tetramethylammonium salt.

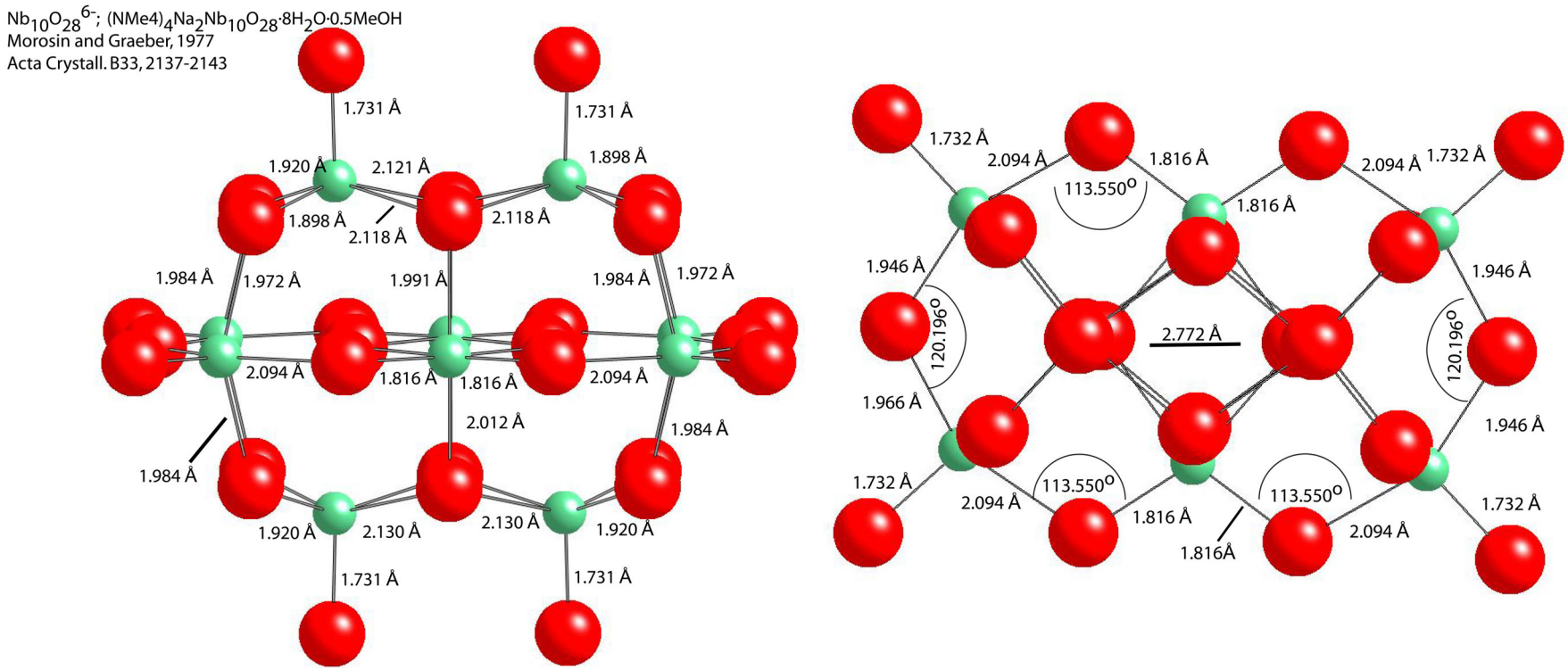

Figure S-5-2: X-ray structural information about the [$Nb_{10}O_{28}^{6-}$] ion from Morosin and Graeber[5] from the sodium tetramethylammonium salt.

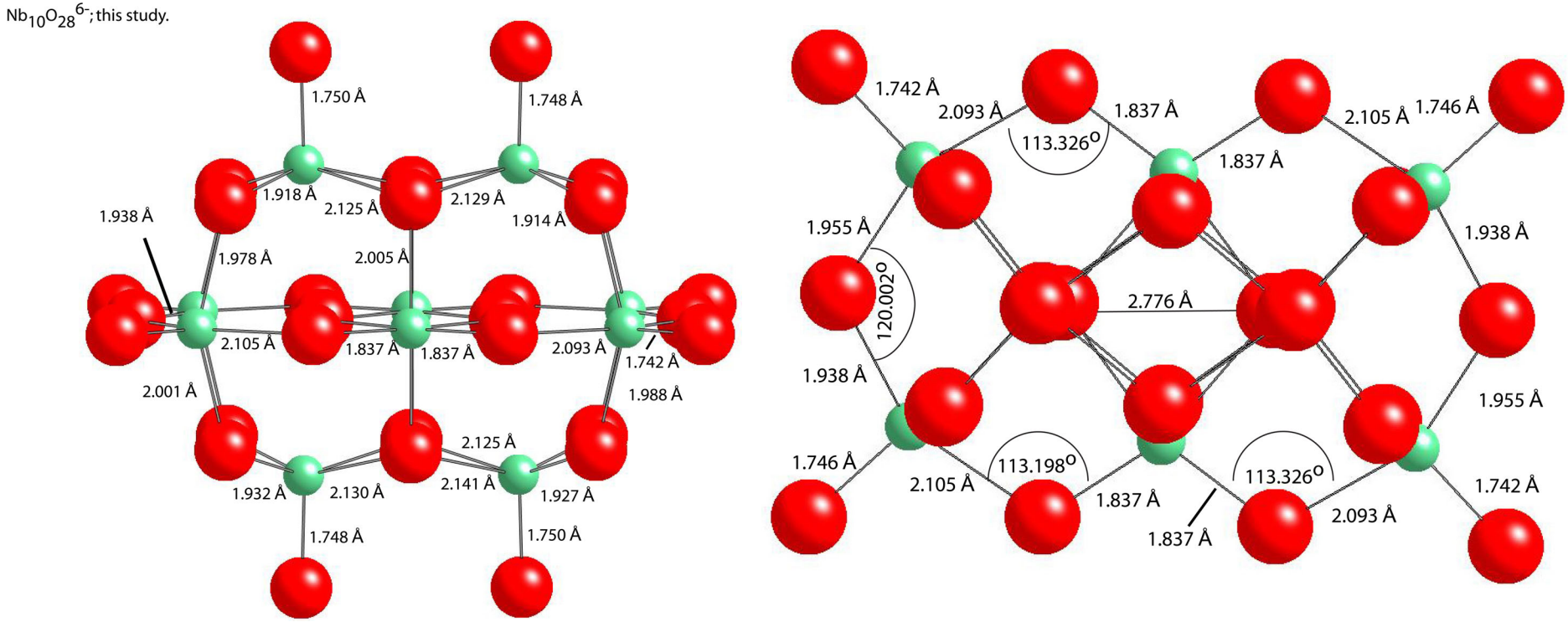

Figure **S-5-C**: Structural details from the $[N(CH_3)_4]_6Nb_{10}O_{28}\cdot 14H_2O$ salt crystals. The structure is deposited with the Fachinformationszentrum Karlsruhe (FIZ, 76344 Eggenstein-Leopoldshafen, Germany) under CSD #419266.

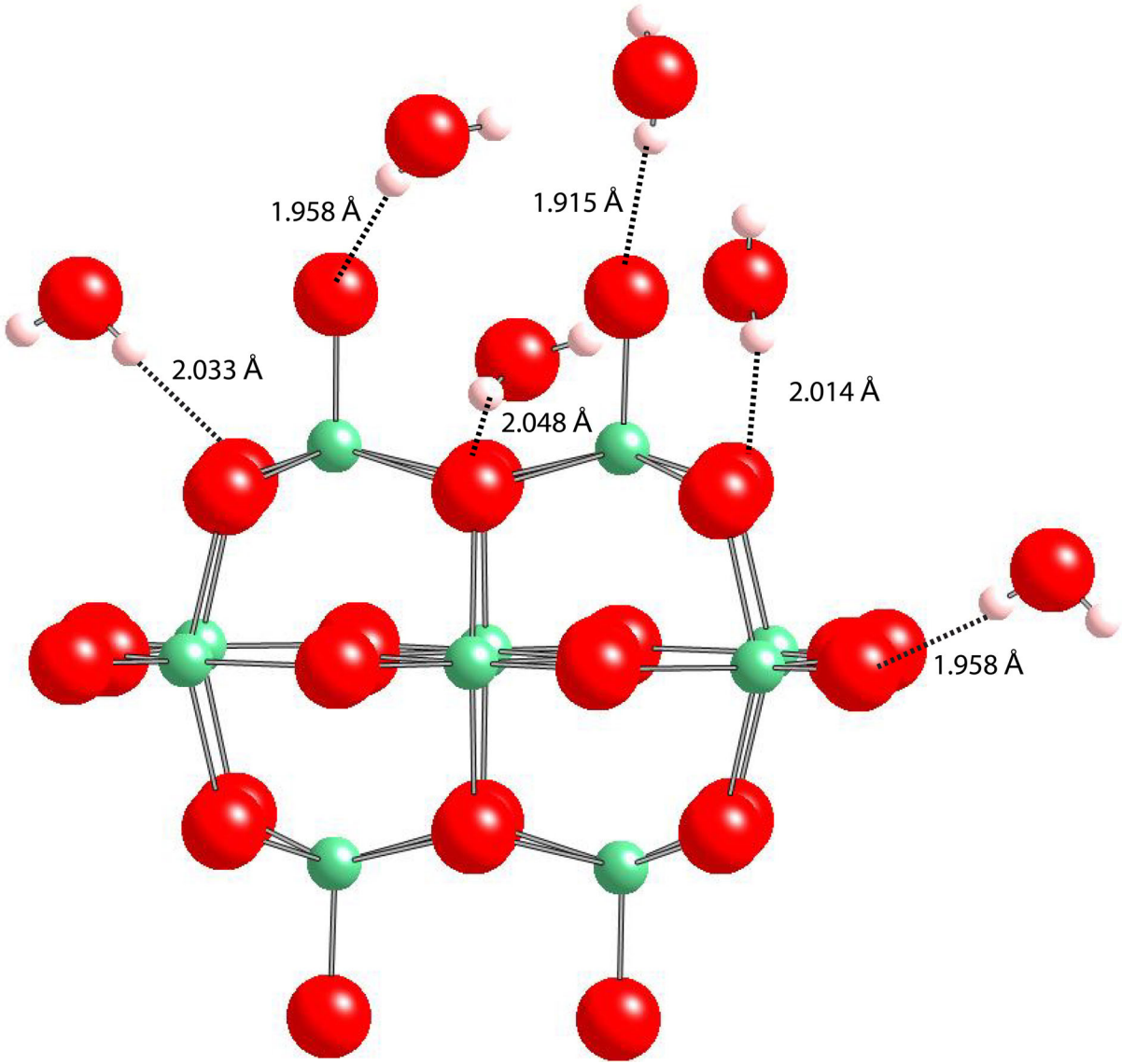

Figure S-5-D. The distribution of hydrogen-bonded waters in the crystallized $[N(CH_3)_4]_6Nb_{10}O_{28}\cdot 14H_2O$ salt. The structure is deposited with the Fachinformationszentrum Karlsruhe (FIZ, 76344 Eggenstein-Leopoldshafen, Germany) under CSD #419266.

References Cited:

[1] K. A. Marek, University of Illinois (Champaign-Urbana), **2001**.

[2] E. Heath, O. W. Howarth, *J. C. S. Dalton* **1981**, 1105.

[3] M. J. Frisch, G. W. Trucks, H. B. Schlegel, G. E. Scuseria, M. A. Robb, J. R. Cheeseman, J. Montgomery, J. A.; , T. Vreven, K. N. Kudin, J. C. Burant, J. M. Millam, S. S. Iyengar, J. Tomasi, V. Barone, B. Mennucci, M. Cossi, G. Scalmani, N. Rega, G. A. Petersson, H. Nakatsuji, M. Hada, M. Ehara, K. Toyota, R. Fukuda, J. Hasegawa, M. Ishida, T. Nakajima, Y. Honda, O. Kitao, H. Nakai, M. Klene, X. Li, J. E. Knox, H. P. Hratchian, J. B. Cross, V. Bakken, C. Adamo, J. Jaramillo, R. Gomperts, R. E. Stratmann, O. Yazyev, A. J. Austin, R. Cammi, C. Pomelli, J. W. Ochterski, P. Y. Ayala, K. Morokuma, G. A. Voth, P. Salvador, J. J. Dannenberg, V. G. Zakrzewski, S. Dapprich, A. D. Daniels, M. C. Strain, O. Farkas, D. K. Malick, A. D. Rabuck, K. Raghavachari, J. B. Foresman, J. V. Ortiz, Q. Cui, A. G. Baboul, S. Clifford, J. Cioslowski, B. B. Stefanov, G. Liu, A. Liashenko, P. Piskorz, I. Komaromi, R. L. Martin, D. J. Fox, T. Keith, M. A. Al-Laham, C. Y. Peng, A. Nanayakkara, M. Challacombe, P. M. W. Gill, B. Johnson, W. Chen, M. W. Wong, C. Gonzalez, J. A. Pople, Gaussian, Inc., Wallingford CT, 2004., **2004**.

[4] X. Lopez, J. A. Fernandez, S. Romo, J. F. Paul, L. Kazansky, J. M. Poblet, *Journal of Computational Chemistry* **2004**, *25*, 1542.

[5] E. J. Graeber, B. Morosin, *Acta Crystallographica B* **1977**, *33*, 2137.